

# Expanded calculations of pn-QRPA electron capture rates on $^{55}\text{Co}$ for presupernova and supernova physics

Jameel-Un Nabi\*      Muhammad Sajjad

## Abstract

Due to its abundance and its relatively high capture rates,  $^{55}\text{Co}$  is one of the key nuclide that can control the dynamics of core collapse of a massive star. Previously we introduced our microscopic calculations of capture rates on  $^{55}\text{Co}$  using the proton-neutron quasi-particle random phase approximation (pn-QRPA) theory. Here we present for the first time an expanded calculation of the electron capture rates on  $^{55}\text{Co}$  on an extensive temperature-density scale. These type of scale is appropriate for interpolation purposes and of greater utility for simulation codes. **PACS:** 26.50.+x, 21.60.Jz, 23.40.-s, 27.40.+z

## 1 Introduction

Supernova explosions are one of the most spectacular explosion in nature when the luminosity of the star becomes comparable to that of an entire galaxy (containing around  $10^{11}$  stars). The supernova outbursts last for very short span of time (several months to a few years) and as such their chance of detection becomes small (once in a few decades)[1]. Massive stars (of masses above  $10M_{\odot}$ ) develop an iron core towards the end of their burning phases. The cores contract to the point that electrons become a degenerate gas. The

---

\*Faculty of Engineering Sciences, GIK Institute of Engineering Sciences and Technology, Topi 23640, Swabi, NWFP, Pakistan. Email: jnabi00@gmail.com

long lasting battle between degeneracy pressure of the electrons and its self-gravity is responsible for further evolution of these stars. When the mass of the core exceeds the corresponding Chandrasekhar limit:

$$M_{Ch} = 1.45(2Y_e^2)M_\odot \quad (1)$$

(here  $Y_e$  is the lepton-to-baryon ratio) the degenerate electron pressure is incapable of opposing self-gravity and rapid contraction of the core is ensued.

Electron capture by free protons and by nuclei tends to decrease the degeneracy pressure and leads to the gravitational collapse of the core of massive stars triggering a supernova explosion. The capture of electrons also plays a key role in the neutronization of the core material, and also effects the formation of heavy elements beyond iron (including the so-called cosmochronometers which provide information about the age of the Galaxy and of the Universe) via the r-process at the final stage of supernova explosion.

The electron capture rates also determine the initial dynamics of the collapse and also, via Eqn. (1), the size of collapsing core and in turn the fate of the shock wave. The electron neutrinos, produced as a result of capture reactions, escape and in turn contribute to the cooling of the iron core. This lowers the entropy of the stellar core and consequently favors the collapse of the core. Bethe et al [2, 3] pointed out that stellar collapse is very sensitive to the entropy of the core and lepton-to-baryon ratio. Fuller, Fowler, and Newman (FFN) [4] performed the first-ever extensive calculation of stellar weak rates including the capture rates, neutrino energy loss rates and decay rates for a wide density and temperature domain. They made this detailed calculations for 226 nuclei in the mass range  $21 \leq A \leq 60$ . They also stressed the importance of the Gamow-Teller (GT) giant resonance strength in the capture of the electron and estimated the GT centroids using zeroth-order ( $0\hbar\omega$ ) shell model.

At the final evolution of the massive star, the electron capture is dominated by Fermi and GT transitions. The treatment of the Fermi transitions, which are important in beta decays, are straightforward while correct description of GT transitions poses a challenging problem in nuclear structure. Later, Aufderheide et al. [5] extended the FFN work for heavier nuclei with  $A > 60$ . They tabulated the 90 top electron capture nuclei averaged throughout the stellar trajectory for  $0.40 \leq Y_e \leq 0.5$  (see Table 25 therein). Since then theoretical efforts were concentrated on the microscopic calculations of capture rates of these iron-regime nuclide. Shell model (e.g. [6]) and

the proton-neutron quasiparticle random phase approximation theory (pn-QRPA) (e.g. [7]) were used extensively and with relative success for the microscopic calculation of stellar capture rates.

Nabi et al. [8] calculated weak interaction rates for 709 nuclei with  $A = 18$  to 100 in stellar matter using the pn-QRPA theory. Since then these calculations were further refined with use of more efficient algorithms, incorporation of latest experimental data, and fine-tuning of model parameters.

$^{55}\text{Co}$  is abundant in the presupernova conditions and is thought to contribute effectively in the notorious dynamics of core-collapse. Aufderheide and collaborators [5] placed  $^{55}\text{Co}$  among the list of top ten most important electron capture nuclei during the presupernova evolution. Later Heger et al. [9] also identified  $^{55}\text{Co}$  as the most important nuclide for electron capture for massive stars ( $25M_{\odot}$ ). Realizing the importance of  $^{55}\text{Co}$  in astrophysical environments, Nabi, Rahman and Sajjad [10] reported the calculation of electron and positron capture rates on  $^{55}\text{Co}$  using the pn-QRPA theory. However there was a need to perform an expanded calculation of these important capture rates on a detailed temperature-density grid suitable for collapse simulation codes. Due to the extreme conditions prevailing in these scenarios, interpolation of calculated rates within large intervals of temperature-density points posed some uncertainty in the values of electron capture rates for collapse simulators.

In this paper we present for the first time an expanded calculation of electron capture rates on  $^{55}\text{Co}$  at suitable intervals of temperature-density intervals. Section 2 deals with the formalism of our calculation. In Section 3 we will be presenting some of our results. We finally will be concluding in Section 4 and at the end Table 3 presents our expanded calculation of Fermi energies and electron capture rates on  $^{55}\text{Co}$  in stellar matter.

## 2 The quasi-particle random phase approximation with a separable interaction

One of the main advantages of using the pn-QRPA theory is the liberty of working the calculations in a huge model space of as big as  $7\hbar\omega$ . We considered a total of 30 excited states in parent nucleus, corresponding to energies in excess of 10 MeV. The inclusion of a very large model space of in our model provides enough space to handle excited states in parent and daughter nuclei

(around 200). Transitions between these states play an important role in the calculated weak rates. For the calculations of these weak rates we made the following assumptions.

- (i) Only allowed GT and super allowed Fermi transitions were calculated. The contribution from forbidden transitions was assumed to be negligible.
- (ii) At high enough temperature, the electron is no more bound to nucleus and the atoms were dealt as being totally ionized with the electrons obeying the Fermi-Dirac distribution.
- (iii) The distortion of electron wave function due to Coulomb interaction with a nucleus was represented by Fermi function in the phase space integrals.
- (iv) We incorporated experimental data for the excitation energies and GT transitions whenever available to add on the reliability of the calculations. The calculated excitation energies (along with their *logft* values) were replaced with the measured one when they were within 0.5 MeV of each other. Missing measured states were inserted. No theoretical levels were replaced (inserted) beyond the level in experimental compilations for  $^{55}\text{Co}$  without definite spin and parity assignment (2.98 MeV).
- (v) Neutrinos and antineutrinos were assumed to escape freely from the interior of star. Neutrino (antineutrino) capture was not taken into account.

We used the quasi-particle proton-neutron random phase approximation (pn-QRPA) with a separable interaction of the form

$$H^{QRPA} = H^{sp} + V^{pair} + V_{GT}^{ph} + V_{GT}^{pp}, \quad (2)$$

here  $H^{sp}$  is the single-particle Hamiltonian,  $V^{pair}$  is the pairing force,  $V_{GT}^{ph}$  is the particle-hole (ph) Gamow-Teller force, and  $V_{GT}^{pp}$  is the particle-particle (pp) Gamow-Teller force. Single particle energies and wave functions were calculated in the Nilsson model, which takes into account nuclear deformations. Pairing was treated in the BCS approximation. The proton-neutron residual interactions occurred as particle-hole and particle-particle interaction. The interactions were given separable form and were characterized by two interaction constants  $\chi$  and  $\kappa$ , respectively. The selections of these two constants were done in an optimal fashion. For details of the fine tuning of the Gamow-Teller strength parameters, we refer to Ref. [11,12]. In this work, we took the values of  $\chi = 0.2\text{MeV}$  and  $\kappa = 0.07\text{MeV}$ . Other parameters required for the calculation of weak rates are the Nilsson potential parameters, the deformation, the pairing gaps, and the Q-value of the reaction. Nilsson-potential parameters were taken from Ref. [13] and the Nilsson oscillator

constant was chosen as  $\hbar\omega = 41A^{-1/3}(MeV)$  (the same for protons and neutrons). The calculated half-lives depend only weakly on the values of the pairing gaps [14]. Thus, the traditional choice of  $\Delta_p = \Delta_n = 12/\sqrt{A}(MeV)$  was applied in the present work. The deformation parameter for  $^{55}\text{Co}$ ,  $\delta$ , was taken to be 0.06, according to Möller and Nix [15]. (See also the discussion on choice of deformation parameter in Ref [16].)

The RPA is formulated for excitations from the  $J^\pi = 0$  ground state of an even-even nucleus. When the parent nucleus has an odd nucleon, the ground state can be expressed as a one-quasiparticle (q.p.) state, in which the odd q.p. occupies the single-q.p. orbit of the smallest energy. Then two types of transitions are possible. One is the phonon excitations, in which the q.p. acts merely as a spectator. The other is transitions of the q.p., where phonon correlations to the q.p. transitions in first order perturbation are introduced [17]. The phonon-correlated one-q.p. states are defined by

$$|p_c\rangle = a_p^+|-\rangle + \sum_{n,\omega} a_n^+ A_\omega^+(\mu)|-\rangle \times \\ |\langle -| [a_n^+ A_\omega^+(\mu)]^+ H_{31} a_p^+|-\rangle E_p(n, \omega), \quad (3a)$$

$$|n_c\rangle = a_n^+|-\rangle + \sum_{p,\omega} a_p^+ A_\omega^+(-\mu)|-\rangle \times \\ \langle -| [a_p^+ A_\omega^+(-\mu)]^+ H_{31} a_n^+|-\rangle E_n(p, \omega), \quad (3b)$$

$$E_a(b, \omega) = \frac{1}{(\varepsilon_a - \varepsilon_b - \omega)} \quad (4)$$

the first term of Eqn. (3) is a proton (neutron) q.p. state and the second term represents correlations of RPA phonons admixed by the phonon-q.p. coupling Hamiltonian  $H_{31}$ , which is obtained from the separable ph and pp forces by the Bogoliubov transformation [18]. The sums run over all phonons and neutron (proton) q.p. states which satisfy  $m_p - m_n = \mu$ , where  $m_{p(n)}$  denotes the third component of the angular momentum and  $\pi_p \cdot \pi_n = 1$ . Derivations of the q.p. transitions amplitudes for the correlated states are given in Ref.[18] for a general force and a general mode of charge-changing transitions. Also

$$\langle n_c | t_\pm \sigma_{-\mu} | p_c \rangle = (-1)^\mu \langle p_c | t_\mp \sigma_\mu | n_c \rangle \quad (5)$$

The excited states can be constructed as phonon-correlated multi-quasiparticles states. The transition amplitudes between the multi-quasiparticle states can

then be reduced to those of single-particle states. Low-lying states of an odd-proton even-neutron nucleus ( $^{55}\text{Co}$ ) can be constructed

(i) by exciting the odd proton from the ground state (one-quasiparticle states),

(ii) by excitation of paired proton (three proton states), or,

(iii) by excitation of a paired neutron (one-proton two-neutron states).

The multi-quasiparticle transitions can be reduced to ones involving correlated (c) one-quasiparticle states:

$$\begin{aligned}
& \langle p_1^f p_2^f n_{1c}^f | t_{\pm} \sigma_{-\mu} | p_1^i p_2^i p_{3c}^i \rangle = \\
& \delta(p_1^f, p_2^i) \delta(p_2^f, p_3^i) \langle n_{1c}^f | t_{\pm} \sigma_{-\mu} | p_{1c}^i \rangle \\
& - \delta(p_1^f, p_1^i) \delta(p_2^f, p_3^i) \langle n_{1c}^f | t_{\pm} \sigma_{-\mu} | p_{2c}^i \rangle \\
& + \delta(p_1^f, p_1^i) \delta(p_2^f, p_2^i) \langle n_{1c}^f | t_{\pm} \sigma_{-\mu} | p_{3c}^i \rangle
\end{aligned} \tag{6}$$

$$\begin{aligned}
& \langle p_1^f p_2^f n_{1c}^f | t_{\pm} \sigma_{\mu} | p_1^i n_1^i n_{2c}^i \rangle = \\
& \delta(n_1^f, n_2^i) \left[ \delta(p_1^f, p_1^i) \langle p_{2c}^f | t_{\pm} \sigma_{\mu} | n_{1c}^i \rangle \right. \\
& \quad \left. - \delta(p_2^f, p_1^i) \langle p_{1c}^f | t_{\pm} \sigma_{\mu} | n_{1c}^i \rangle \right] - \delta(n_1^f, n_1^i) \\
& \times \left[ \delta(p_1^f, p_1^i) \langle p_{2c}^f | t_{\pm} \sigma_{\mu} | n_{2c}^i \rangle - \delta(p_2^f, p_1^i) \right. \\
& \quad \left. \times \langle p_{1c}^f | t_{\pm} \sigma_{\mu} | n_{2c}^i \rangle \right]
\end{aligned} \tag{7}$$

$$\begin{aligned}
& \langle n_1^f n_2^f n_{3c}^f | t_{\pm} \sigma_{-\mu} | p_1^i n_1^i n_{2c}^i \rangle = \\
& \delta(n_2^f, n_1^i) \delta(n_3^f, n_2^i) \langle n_{1c}^f | t_{\pm} \sigma_{-\mu} | p_{1c}^i \rangle \\
& - \delta(n_1^f, n_1^i) \delta(n_3^f, n_2^i) \langle n_{2c}^f | t_{\pm} \sigma_{-\mu} | p_{1c}^i \rangle \\
& + \delta(n_1^f, n_1^i) \delta(n_2^f, n_2^i) \langle n_{3c}^f | t_{\pm} \sigma_{-\mu} | p_{1c}^i \rangle.
\end{aligned} \tag{8}$$

For the case of daughter nucleus ( $^{55}\text{Fe}$ ), which is an odd-neutron even-proton nucleus, the excited states can be constructed

- (i) by lifting the odd neutron from the ground state to excited states (one quasiparticle states),
  - (ii) by excitation of a paired neutron (three neutron states), or,
  - (iii) by the excitation of a paired proton (one-neutron two-proton states).
- Once again the multi-qp states are reduced to ones involving only correlated (c) one-qp states:

$$\begin{aligned}
& \langle p_1^f n_1^f n_{2c}^f | t_{\pm} \sigma_{\mu} | n_1^i n_2^i n_{3c}^i \rangle = \\
& \delta(n_1^f, n_2^i) \delta(n_2^f, n_3^i) \langle p_{1c}^f | t_{\pm} \sigma_{\mu} | n_{1c}^i \rangle \\
& - \delta(n_1^f, n_1^i) \delta(n_2^f, n_3^i) \langle p_{1c}^f | t_{\pm} \sigma_{\mu} | n_{2c}^i \rangle \\
& + \delta(n_1^f, n_1^i) \delta(n_2^f, n_2^i) \langle p_{1c}^f | t_{\pm} \sigma_{\mu} | n_{3c}^i \rangle
\end{aligned} \tag{9}$$

$$\begin{aligned}
& \langle p_1^f n_1^f n_{2c}^f | t_{\pm} \sigma_{-\mu} | p_1^i p_2^i n_{1c}^i \rangle = \\
& \delta(p_1^f, p_2^i) \left[ \delta(n_1^f, n_1^i) \langle n_{2c}^f | t_{\pm} \sigma_{-\mu} | p_{1c}^i \rangle \right. \\
& - \delta(n_2^f, n_1^i) \langle n_{1c}^f | t_{\pm} \sigma_{-\mu} | p_{1c}^i \rangle - \delta(p_1^f, p_1^i) \\
& \times \left[ \delta(n_1^f, n_1^i) \langle n_{2c}^f | t_{\pm} \sigma_{-\mu} | p_{2c}^i \rangle - \delta(n_2^f, n_1^i) \right. \\
& \left. \left. \times \langle n_{1c}^f | t_{\pm} \sigma_{-\mu} | p_{2c}^i \rangle \right] \right].
\end{aligned} \tag{10}$$

$$\begin{aligned}
& \langle p_1^f p_2^f p_{3c}^f | t_{\pm} \sigma_{\mu} | p_1^i p_2^i n_{1c}^i \rangle = \\
& \delta(p_2^f, p_1^i) \delta(p_3^f, p_2^i) \langle p_{1c}^f | t_{\pm} \sigma_{\mu} | n_{1c}^i \rangle \\
& - \delta(p_1^f, p_1^i) \delta(p_3^f, p_2^i) \langle p_{2c}^f | t_{\pm} \sigma_{\mu} | n_{1c}^i \rangle \\
& + \delta(p_1^f, p_1^i) \delta(p_2^f, p_2^i) \langle p_{3c}^f | t_{\pm} \sigma_{\mu} | n_{1c}^i \rangle.
\end{aligned} \tag{11}$$

For all the given q.p. transition amplitudes [Eqs. (6)- (11)], the antisymmetrization of the single- q.p. states was taken into account:  
 $p_1^f < p_2^f < p_3^f < p_4^f$ ,

$$\begin{aligned}
n_1^f &< n_2^f < n_3^f < n_4^f, \\
p_1^i &< p_2^i < p_3^i < p_4^i, \\
n_1^i &< n_2^i < n_3^i < n_4^i.
\end{aligned}$$

GT transitions of phonon excitations for every excited state were also taken into account. We also assumed that the quasiparticles in the parent nucleus remained in the same quasiparticle orbits.

The capture rates of a transition from the  $i$ th state of the parent to the  $j$ th state of the daughter nucleus is given by

$$\lambda_{ij}^{ec} = \left[ \frac{\ln 2}{D} \right] [f_{ij}(T, \rho, E_f)] \left[ B(F)_{ij} + \left( g_A/g_V \right)^2 B(GT)_{ij} \right]. \quad (12)$$

We took the value of  $D=6295$ s [19] and the ratio of the axial vector to the vector coupling constant as  $-1.254$  [20].  $B'_{ij}$ s are the sum of reduced transition probabilities of the Fermi B(F) and GT transitions B(GT). Details of these reduced transition probabilities can be found in Ref. [7, 21]. The phase space integral  $f_{ij}$  is an integral over total energy and for electron capture it is given by

$$f_{ij} = \int_{w_i}^{\infty} w \sqrt{w^2 - 1} (w_m + w)^2 F(+Z, w) G_- dw. \quad (13)$$

In above equation  $w$  is the total energy of the electron including its rest mass,  $w_i$  is the total capture threshold energy (rest+kinetic) for electron capture.  $F(+Z, w)$  are the Fermi functions and were calculated according to the procedure adopted by Gove and Martin [22].  $G_-$  is the Fermi-Dirac distribution function for electrons,

$$G_- = \left[ \exp \left( \frac{E - E_f}{kT} \right) + 1 \right]^{-1}. \quad (14)$$

Here  $E = (w - 1)$  is the kinetic energy of the electrons,  $E_f$  is the Fermi energy of the electrons,  $T$  is the temperature, and  $k$  is the Boltzmann constant.

The number density of electrons associated with protons and nuclei is  $\rho Y_e N_A$  ( $\rho$  is the baryon density and  $N_A$  is Avogadro's number) where,

$$\rho Y_e = \frac{1}{\pi^2 N_A} \left( \frac{m_e c}{\hbar} \right)^3 \int_0^{\infty} (G_- - G_+) p^2 dp, \quad (15)$$

here  $p = (w^2 - 1)^{1/2}$  is the electron momentum and Eqn. (15) has the units of  $mol \text{ cm}^{-3}$ .  $G_+$  is the Fermi-Dirac distribution function for positrons,

$$G_+ = \left[ \exp \left( \frac{E + 2 + E_f}{kT} \right) + 1 \right]^{-1}. \quad (16)$$

Eqn. (15) is used for an iterative calculation of Fermi energies for selected values of  $Y_e$  and  $T$ . There is a finite probability of occupation of parent excited states in the stellar environment as result of the high temperature in the interior of massive stars. Capture rates then also have a finite contribution from these excited states. The total electron capture rate per unit time per nucleus is given by

$$\lambda_{ec} = \sum_{ij} P_i \lambda_{ij}. \quad (17)$$

The summation over all initial and final states was carried out until satisfactory convergence in the rate calculations was achieved. Here  $P_i$  is the probability of occupation of parent excited states and follows the normal Boltzmann distribution.

### 3 Results and discussions

The luxury of having a huge model space at our disposal allowed us to perform the calculation of electron capture rates from 30 excited states of  $^{55}\text{Co}$ . At temperatures pertinent to supernova environment we have a finite probability of occupation of excited states and a microscopic calculation of rates from these excited states is desirable. Earlier, Nabi and Sajjad [16] did point to the fact that the Brink's hypothesis ( and back resonances for calculation of beta decay rates) usually employed in large-scale shell model calculations is not a good approximation to use in stellar rate calculations. Brink's hypothesis states that GT strength distribution on excited states is identical to that from ground state, shifted only by the excitation energy of the state whereas the GT back resonances are states reached by the strong GT transitions in the electron capture process built on ground and excited states. Table 1 shows the calculated excited states of  $^{55}\text{Co}$  using the pn-QRPA theory. For each parent state we considered around 200 excited states in daughter  $^{55}\text{Fe}$ .

The GT strength distribution from ground state and first two excited states of  $^{55}\text{Co}$  was presented earlier (see Fig.1 of Ref [10]). We calculated the total GT strength from ground state to be 7.4 with a centroid in the energy range 7.1 - 7.4 MeV in daughter  $^{55}\text{Fe}$ . Table 2 shows the calculated B(GT)

strength values for the ground state of  $^{55}\text{Co}$ . The strengths are given up to energy of 10 MeV in daughter nucleus,  $^{55}\text{Fe}$ . Calculated B(GT) strength of magnitude less than  $10^{-3}$  are not included in this table.

Comparison of our calculation of electron capture rates with the pioneer work of FFN [4] and large-scale shell model calculations [23] was also presented in detail in Ref [10]. The pn-QRPA rates were enhanced up to two orders of magnitude compared to the large-scale shell model calculations. Our rates were also enhanced as compared to the FFN calculations. However at high temperatures and densities(  $\log T > 9.4$ ;  $\rho \approx 10^{11} gcm^{-3}$ ) the FFN rates surpass our rates. The main reason for this enhancement was that FFN placed the GT centroid at too low excitation energies [10, 23].

Fig.1 shows four panels depicting our calculated electron capture rates at selected temperature and density domain. The upper left panel shows the electron capture rates in low-density region ( $\rho[gcm^{-3}] = 10^{0.5}, 10^{1.5}$  and  $10^{2.5}$ ), the upper right in medium-low density region ( $\rho[gcm^{-3}] = 10^{3.5}, 10^{4.5}$  and  $10^{5.5}$ ), the lower left in medium-high density region ( $\rho[gcm^{-3}] = 10^{6.5}, 10^{7.5}$  and  $10^{8.5}$ ) and finally the lower right panel depicts our calculated electron capture rates in high density region ( $\rho[gcm^{-3}] = 10^{9.5}, 10^{10.5}$  and  $10^{11}$ ). It can be seen from this figure that in the low density region the capture rates, as a function of temperature, are more or less superimposed on one another. This means that there is no appreciable change in the rates with increasing the density by an order of magnitude. However as we go from the medium low density region to high density region these rates start to 'peel off' from one another. Orders of magnitude difference in rates are observed (as a function of density) in high density regions. For a given density the rates increase monotonically with increasing temperatures. We also notice that the rates coincide at  $T_9 = 30\text{K}$  except for the high density region (where  $T_9$  gives the stellar temperature in units of  $10^9\text{K}$ ).

Fig.2 shows our summed GT strength as a function of excited states in the daughter  $^{55}\text{Fe}$ . We note that almost all the strength cumulates up to an energy around 12 MeV in  $^{55}\text{Fe}$ . No appreciable strength is seen in  $^{55}\text{Fe}$  at higher excitation energies.

We finally present our calculated electron capture rates on a detailed temperature-density grid in Table 3. Here Column 1 shows the density in logarithmic scales (in units of  $gcm^{-3}$ ), Column 2, the stellar temperature in units of  $10^9 K$ , Column 3 gives the calculated Fermi energy at the corresponding temperature and density whereas Column 4 displays the calculated electron capture rates in logarithmic scales (in units of  $sec^{-1}$ ). Tables of rate

calculations presented earlier in compilations (e.g. [24, 7, 4]) were not presented on a detail temperature-density grid and at times lead to erroneous results when interpolated. We hope that this table will prove more useful for core-collapse simulators.

## 4 Conclusions

$^{55}\text{Co}$  is advocated to play a key role amongst the iron-regime nuclide controlling the dynamics of core-collapse of massive stars. The electron capture rates on  $^{55}\text{Co}$  are used as nuclear physics input parameter for core-collapse simulations. Reliable and detailed calculation of electron capture rates is desirable for these codes. These parameters may fine tune the final outcome of these simulations.

Here we present, for the first time, an expanded calculation of stellar electron capture rates on a fine temperature-density scale suitable for simulation codes. We considered a total of 30 parent excited states for the microscopic calculation of these stellar capture rates on  $^{55}\text{Co}$ . Our calculations point towards an enhanced capture rate for  $^{55}\text{Co}$  as compared to large-scale shell model calculations. This may have a significant impact on the outcome of simulation results. We remind the readers that it was the rather reduced electron capture rates on  $^{55}\text{Co}$  (from previous calculations) in the outer layers of the core of massive stars that lead to slowing of the collapse and resulted, consequently, in a large shock radius to deal with [25]. Can our (relatively enhanced) electron capture change this scenario? It might. We again recall that according to the calculations of Aufderheide and collaborators [5], the rate of change of lepton fraction can change by as much as 50 % alone due to electron capture rates on  $^{55}\text{Co}$ . We will urge core-collapse simulators to test run our reported electron capture rates presented here to check for some interesting outcome.

## References

- [1] [1] Dina Prialnik, *An Introduction to the theory of stellar structure and evolution* (Cambridge University Press, Cambridge, 2000).
- [2] [2] H.A. Bethe, G. E. Brown, J. Applegate, and J. M. Lattimer, *Nucl. Phys.* **A324**, 487 (1979).

- [3] [3] H.A. Bethe, Rev. Mod. Phys. **62**, 801 (1990).
- [4] [4] G. M. Fuller, W. A. Fowler, M. J. Newman, Astrophys. J. Suppl. Ser **42**, 447 (1980); **48**, 279 (1982); Astrophys. J. **252**, 715 (1982); **293**, 1 (1985).
- [5] [5] M. B. Aufderheide, I. Fushiki, S. E. Woosley, E. Stanford, and D. H. Hartmann, Astrophys. J. Suppl. **91**, 389 (1994).
- [6] [6] E. Caurier, K. Langanke, G. Martinez-Pinedo, F. Nowacki, Nucl. Phys. **A653**, 439 (1999).
- [7] [7] J.-U. Nabi, H. V. Klapdor-Kleingrothaus, At. Data Nucl. Data Tables **88**, 237 (2004).
- [8] [8] J.-U. Nabi, H. V. Klapdor-Kleingrothaus, Eur. Phys. J. **A5**, 337 (1999).
- [9] [9] A. Heger, K. Langanke, G. Martinez-Pinedo, and S. E. Woosley, Phys. Rev. Lett. **86**, 1678 (2001).
- [10] [10] J.-U. Nabi, M.-U. Rahman and M. Sajjad, Braz. Jour. Phys. **37**, 1 (2007).
- [11] [11] A. Staudt, E. Bender, K. Muto, H.V. Klapdor-Kleingrothaus, At. Data Nucl. Data Tables **44**, 79 (1990).
- [12] [12] M. Hirsch, A. Staudt, K. Muto, H.V. Klapdor-Kleingrothaus, At. Data Nucl. Data Tables **53**, 165 (1993).
- [13] [13] I. Ragnarsson, R. K. Sheline, Phys. Scr. **29**, 385 (1984).
- [14] [14] M. Hirsch, A. Staudt, K. Muto, H.V. Klapdor-Kleingrothaus, Nucl. Phys. **A535**, 62 (1991).
- [15] [15] P. Möller, J. R. Nix, At. Data Nucl. Data Tables **26**, 165 (1981).
- [16] [16] J.-U. Nabi, M. Sajjad, Phys. Rev. **C 76**, 055803 (2007).
- [17] [17] J. A. Halbleib, R. A. Sorensen, Nucl. Phys. **A98**, 542 (1967).
- [18] [18] K. Muto, E. Bender, H. V. Klapdor-Kleingrothaus, Z. Phys. A **334**, 187 (1989).

- [19] [19] G. P. Yost *et al.* (Particle Data Group), Phys. Lett. **B204**, 1 (1988).
- [20] [20] V. Rodin, A. Faessler, F. Simkovic, and P. Vogel, Czech. J. Phys. **56**, 495 (2006).
- [21] [21] J.-U. Nabi and M.-U. Rahman, Phys. Lett. **B612**, 190 (2005).
- [22] [22] N. B. Gove, M. J. Martin, At. Data Nucl. Data Tables **10**, 205 (1971).
- [23] [23] K. Langanke, G. Martinez-Pinedo, Phys. Lett. **B436**, 19 (1998).
- [24] [24] J.-U. Nabi, H. V. Klapdor-Kleingrothaus, At. Data Nucl. Data Tables **71**, 149 (1999).
- [25] [25] W. R. Hix, O. E. Messer, A. Mezzacappa, M. Liebendrfer, J. Sampo, K. Langanke, D. J. Dean, and G. Martínez-Pinedo, Phys. Rev. Lett. **91**, 201102 (2003).

**Table 1:** Calculated excited states in parent  $^{55}\text{Co}$ .

0.0	2.17	2.57	2.92	3.08	3.30	3.87	4.10	4.48	4.89
5.20	5.47	5.68	5.99	6.20	6.50	6.79	7.08	7.33	7.65
7.88	8.16	8.42	8.67	8.96	9.21	9.48	9.74	9.89	10.00

**Table 2:** Calculated B(GT+) values from ground state in  $^{55}\text{Co}$ .

Energy(MeV)	B(GT+)	Energy(MeV)	B(GT+)	Energy(MeV)	B(GT+)
2.46	2.35E-01	6.36	5.45E-01	8.25	1.06E-01
3.01	2.13E-01	6.66	3.22E-01	8.36	2.06E-03
3.45	3.05E-01	6.85	1.70E-01	8.62	8.83E-03
3.57	4.50E-03	7.00	2.01E-03	8.73	2.58E-02
3.68	1.84E-01	7.14	8.70E-01	8.90	2.45E-02
3.90	2.52E-01	7.43	7.07E-01	9.11	1.38E-02
4.11	2.50E-02	7.59	1.87E-02	9.26	3.04E-02
5.82	2.94E-01	7.76	3.89E-01	9.42	1.52E-02
5.93	2.60E-03	7.92	1.49E-02	9.60	1.70E-02
6.13	1.98E-01	8.04	1.69E-01		

**Table 3:** Calculated electron rates on  $^{55}\text{Co}$  for different selected densities and temperatures in stellar matter. ADen is the  $\log(\rho Y_e)$  and has units of  $g\text{cm}^{-3}$ , where  $\rho$  is the baryon density and  $Y_e$  is the ratio of the electron number to the baryon number. Temperatures ( $T_9$ ) are measured in  $10^9$  K. EFermi is the total Fermi energy of electron including the rest mass (MeV). E-Cap are the electron capture rates. The calculated electron capture rates are tabulated in  $\log_{10}\lambda_{ec}$  in units of  $\text{sec}^{-1}$ .

ADen	$T_9$	EFermi	E-Cap	ADen	$T_9$	EFermi	E-Cap	ADen	$T_9$	EFermi	E-Cap
0.5	0.5	0.065	-8.726	1	8.5	0	-0.97	2	4.5	0	-2.44
0.5	1	0	-6.321	1	9	0	-0.824	2	5	0	-2.206
0.5	1.5	0	-5.068	1	9.5	0	-0.681	2	5.5	0	-1.994
0.5	2	0	-4.308	1	10	0	-0.541	2	6	0	-1.798
0.5	2.5	0	-3.766	1	15	0	0.683	2	6.5	0	-1.615
0.5	3	0	-3.344	1	20	0	1.601	2	7	0	-1.443
0.5	3.5	0	-2.997	1	25	0	2.284	2	7.5	0	-1.279
0.5	4	0	-2.701	1	30	0	2.813	2	8	0	-1.122
0.5	4.5	0	-2.44	1.5	0.5	0.162	-7.747	2	8.5	0	-0.97
0.5	5	0	-2.207	1.5	1	0.002	-6.314	2	9	0	-0.823
0.5	5.5	0	-1.994	1.5	1.5	0	-5.068	2	9.5	0	-0.68
0.5	6	0	-1.798	1.5	2	0	-4.307	2	10	0	-0.541
0.5	6.5	0	-1.616	1.5	2.5	0	-3.765	2	15	0	0.683
0.5	7	0	-1.443	1.5	3	0	-3.344	2	20	0	1.601
0.5	7.5	0	-1.279	1.5	3.5	0	-2.997	2	25	0	2.285
0.5	8	0	-1.122	1.5	4	0	-2.7	2	30	0	2.813
0.5	8.5	0	-0.971	1.5	4.5	0	-2.44	2.5	0.5	0.261	-6.748
0.5	9	0	-0.824	1.5	5	0	-2.206	2.5	1	0.015	-6.246
0.5	9.5	0	-0.681	1.5	5.5	0	-1.994	2.5	1.5	0.002	-5.064
0.5	10	0	-0.542	1.5	6	0	-1.798	2.5	2	0	-4.306
0.5	15	0	0.682	1.5	6.5	0	-1.615	2.5	2.5	0	-3.765
0.5	20	0	1.6	1.5	7	0	-1.443	2.5	3	0	-3.344
0.5	25	0	2.283	1.5	7.5	0	-1.279	2.5	3.5	0	-2.997
0.5	30	0	2.812	1.5	8	0	-1.122	2.5	4	0	-2.7
1	0.5	0.113	-8.245	1.5	8.5	0	-0.97	2.5	4.5	0	-2.439
1	1	0	-6.32	1.5	9	0	-0.823	2.5	5	0	-2.206
1	1.5	0	-5.069	1.5	9.5	0	-0.68	2.5	5.5	0	-1.994
1	2	0	-4.307	1.5	10	0	-0.541	2.5	6	0	-1.798
1	2.5	0	-3.765	1.5	15	0	0.683	2.5	6.5	0	-1.615
1	3	0	-3.344	1.5	20	0	1.601	2.5	7	0	-1.443
1	3.5	0	-2.997	1.5	25	0	2.285	2.5	7.5	0	-1.279
1	4	0	-2.7	1.5	30	0	2.813	2.5	8	0	-1.122
1	4.5	0	-2.44	2	0.5	0.212	-7.248	2.5	8.5	0	-0.97
1	5	0	-2.206	2	1	0.005	-6.298	2.5	9	0	-0.823
1	5.5	0	-1.994	2	1.5	0	-5.067	2.5	9.5	0	-0.68
1	6	0	-1.798	2	2	0	-4.307	2.5	10	0	-0.541
1	6.5	0	-1.615	2	2.5	0	-3.765	2.5	15	0	0.683
1	7	0	-1.443	2	3	0	-3.344	2.5	20	0	1.601
1	7.5	0	-1.279	2 15	3.5	0	-2.997	2.5	25	0	2.285
1	8	0	-1.122	2	4	0	-2.7	2.5	30	0	2.813

ADen	$T_9$	EFermi	E-Cap	ADen	$T_9$	EFermi	E-Cap	ADen	$T_9$	EFermi	E-Cap
3	0.5	0.311	-6.248	4	0.5	0.411	-5.252	5	0.5	0.522	-4.281
3	1	0.046	-6.092	4	1	0.209	-5.274	5	1	0.413	-4.282
3	1.5	0.005	-5.053	4	1.5	0.047	-4.912	5	1.5	0.265	-4.193
3	2	0.001	-4.304	4	2	0.014	-4.273	5	2	0.128	-3.989
3	2.5	0.001	-3.764	4	2.5	0.006	-3.753	5	2.5	0.062	-3.643
3	3	0	-3.343	4	3	0.004	-3.338	5	3	0.035	-3.286
3	3.5	0	-2.996	4	3.5	0.002	-2.994	5	3.5	0.023	-2.965
3	4	0	-2.7	4	4	0.002	-2.698	5	4	0.016	-2.68
3	4.5	0	-2.439	4	4.5	0.001	-2.438	5	4.5	0.012	-2.427
3	5	0	-2.206	4	5	0.001	-2.205	5	5	0.009	-2.197
3	5.5	0	-1.994	4	5.5	0.001	-1.993	5	5.5	0.007	-1.987
3	6	0	-1.798	4	6	0.001	-1.797	5	6	0.006	-1.793
3	6.5	0	-1.615	4	6.5	0.001	-1.614	5	6.5	0.005	-1.611
3	7	0	-1.443	4	7	0	-1.442	5	7	0.004	-1.44
3	7.5	0	-1.279	4	7.5	0	-1.278	5	7.5	0.004	-1.276
3	8	0	-1.122	4	8	0	-1.121	5	8	0.003	-1.12
3	8.5	0	-0.97	4	8.5	0	-0.97	5	8.5	0.003	-0.969
3	9	0	-0.823	4	9	0	-0.823	5	9	0.002	-0.822
3	9.5	0	-0.68	4	9.5	0	-0.68	5	9.5	0.002	-0.679
3	10	0	-0.541	4	10	0	-0.541	5	10	0.002	-0.54
3	15	0	0.683	4	15	0	0.683	5	15	0.001	0.683
3	20	0	1.601	4	20	0	1.601	5	20	0	1.601
3	25	0	2.285	4	25	0	2.285	5	25	0	2.285
3	30	0	2.813	4	30	0	2.813	5	30	0	2.813
3.5	0.5	0.361	-5.749	4.5	0.5	0.464	-4.76	5.5	0.5	0.598	-3.819
3.5	1	0.115	-5.745	4.5	1	0.309	-4.778	5.5	1	0.528	-3.79
3.5	1.5	0.015	-5.018	4.5	1.5	0.13	-4.637	5.5	1.5	0.423	-3.7
3.5	2	0.004	-4.296	4.5	2	0.044	-4.199	5.5	2	0.295	-3.585
3.5	2.5	0.002	-3.761	4.5	2.5	0.02	-3.726	5.5	2.5	0.18	-3.412
3.5	3	0.001	-3.342	4.5	3	0.011	-3.325	5.5	3	0.11	-3.165
3.5	3.5	0.001	-2.996	4.5	3.5	0.007	-2.987	5.5	3.5	0.072	-2.896
3.5	4	0.001	-2.699	4.5	4	0.005	-2.694	5.5	4	0.05	-2.638
3.5	4.5	0	-2.439	4.5	4.5	0.004	-2.435	5.5	4.5	0.038	-2.399
3.5	5	0	-2.206	4.5	5	0.003	-2.203	5.5	5	0.029	-2.178
3.5	5.5	0	-1.993	4.5	5.5	0.002	-1.992	5.5	5.5	0.023	-1.973
3.5	6	0	-1.797	4.5	6	0.002	-1.796	5.5	6	0.019	-1.782
3.5	6.5	0	-1.615	4.5	6.5	0.002	-1.614	5.5	6.5	0.016	-1.603
3.5	7	0	-1.442	4.5 <sub>16</sub>	7	0.001	-1.442	5.5	7	0.013	-1.433
3.5	7.5	0	-1.279	4.5	7.5	0.001	-1.278	5.5	7.5	0.012	-1.271
3.5	8	0	-1.122	4.5	8	0.001	-1.121	5.5	8	0.01	-1.116
3.5	8.5	0	-0.97	4.5	8.5	0.001	-0.97	5.5	8.5	0.009	-0.965
3.5	9	0	-0.823	4.5	9	0.001	-0.823	5.5	9	0.008	-0.819
3.5	9.5	0	-0.68	4.5	9.5	0.001	-0.68	5.5	9.5	0.007	-0.677
3.5	10	0	-0.541	4.5	10	0.001	-0.541	5.5	10	0.006	-0.538

ADen	$T_9$	EFermi	E-Cap	ADen	$T_9$	EFermi	E-Cap	ADen	$T_9$	EFermi	E-Cap
6	0.5	0.713	-3.352	7	0.5	1.217	-2.228	8	0.5	2.444	-0.744
6	1	0.672	-3.297	7	1	1.2	-2.172	8	1	2.437	-0.709
6	1.5	0.604	-3.195	7	1.5	1.173	-2.076	8	1.5	2.424	-0.646
6	2	0.512	-3.091	7	2	1.133	-1.982	8	2	2.406	-0.587
6	2.5	0.405	-2.987	7	2.5	1.083	-1.901	8	2.5	2.383	-0.538
6	3	0.299	-2.861	7	3	1.021	-1.827	8	3	2.355	-0.495
6	3.5	0.214	-2.699	7	3.5	0.95	-1.757	8	3.5	2.322	-0.457
6	4	0.156	-2.51	7	4	0.871	-1.688	8	4	2.283	-0.419
6	4.5	0.117	-2.312	7	4.5	0.785	-1.617	8	4.5	2.24	-0.382
6	5	0.091	-2.117	7	5	0.698	-1.542	8	5	2.192	-0.344
6	5.5	0.073	-1.929	7	5.5	0.613	-1.46	8	5.5	2.139	-0.304
6	6	0.06	-1.749	7	6	0.534	-1.369	8	6	2.081	-0.263
6	6.5	0.05	-1.577	7	6.5	0.465	-1.269	8	6.5	2.019	-0.22
6	7	0.042	-1.413	7	7	0.404	-1.163	8	7	1.952	-0.174
6	7.5	0.036	-1.255	7	7.5	0.353	-1.05	8	7.5	1.882	-0.126
6	8	0.032	-1.102	7	8	0.31	-0.933	8	8	1.808	-0.074
6	8.5	0.028	-0.954	7	8.5	0.274	-0.813	8	8.5	1.732	-0.019
6	9	0.025	-0.81	7	9	0.244	-0.691	8	9	1.653	0.039
6	9.5	0.022	-0.669	7	9.5	0.218	-0.569	8	9.5	1.574	0.101
6	10	0.02	-0.531	7	10	0.196	-0.445	8	10	1.493	0.166
6	15	0.009	0.686	7	15	0.085	0.711	8	15	0.817	0.946
6	20	0.005	1.603	7	20	0.047	1.613	8	20	0.47	1.716
6	25	0.003	2.285	7	25	0.03	2.291	8	25	0.301	2.344
6	30	0.002	2.813	7	30	0.021	2.816	8	30	0.209	2.847
6.5	0.5	0.905	-2.834	7.5	0.5	1.705	-1.524	8.5	0.5	3.547	0.075
6.5	1	0.88	-2.772	7.5	1	1.693	-1.479	8.5	1	3.542	0.103
6.5	1.5	0.837	-2.667	7.5	1.5	1.675	-1.398	8.5	1.5	3.534	0.154
6.5	2	0.777	-2.564	7.5	2	1.648	-1.322	8.5	2	3.521	0.202
6.5	2.5	0.701	-2.471	7.5	2.5	1.614	-1.257	8.5	2.5	3.506	0.24
6.5	3	0.612	-2.384	7.5	3	1.573	-1.199	8.5	3	3.487	0.271
6.5	3.5	0.517	-2.293	7.5	3.5	1.524	-1.145	8.5	3.5	3.464	0.299
6.5	4	0.424	-2.191	7.5	4	1.468	-1.093	8.5	4	3.438	0.326
6.5	4.5	0.343	-2.071	7.5	4.5	1.405	-1.04	8.5	4.5	3.408	0.352
6.5	5	0.277	-1.937	7.5	5	1.336	-0.987	8.5	5	3.375	0.379
6.5	5.5	0.226	-1.794	7.5	5.5	1.262	-0.933	8.5	5.5	3.339	0.406
6.5	6	0.187	-1.646	7.5	6	1.183	-0.876	8.5	6	3.299	0.436
6.5	6.5	0.157	-1.497	7.5	6.5	1.101	-0.816	8.5	6.5	3.256	0.467
6.5	7	0.134	-1.35	7.5 <sub>17</sub>	7	1.018	-0.752	8.5	7	3.209	0.5
6.5	7.5	0.115	-1.204	7.5	7.5	0.937	-0.683	8.5	7.5	3.159	0.536
6.5	8	0.1	-1.061	7.5	8	0.858	-0.608	8.5	8	3.106	0.575
6.5	8.5	0.088	-0.92	7.5	8.5	0.783	-0.527	8.5	8.5	3.05	0.616
6.5	9	0.078	-0.781	7.5	9	0.714	-0.441	8.5	9	2.99	0.661
6.5	9.5	0.069	-0.645	7.5	9.5	0.651	-0.35	8.5	9.5	2.928	0.708
6.5	10	0.062	-0.51	7.5	10	0.593	-0.254	8.5	10	2.863	0.759

ADen	$T_9$	EFermi	E-Cap	ADen	$T_9$	EFermi	E-Cap	ADen	$T_9$	EFermi	E-Cap
9	0.5	5.179	0.946	9.5	8.5	7.351	2.179	10.5	4.5	16.28	3.907
9	1	5.176	0.969	9.5	9	7.323	2.201	10.5	5	16.273	3.911
9	1.5	5.17	1.012	9.5	9.5	7.293	2.225	10.5	5.5	16.265	3.915
9	2	5.162	1.051	9.5	10	7.261	2.252	10.5	6	16.256	3.919
9	2.5	5.151	1.082	9.5	15	6.86	2.627	10.5	6.5	16.247	3.923
9	3	5.138	1.107	9.5	20	6.307	3.018	10.5	7	16.237	3.928
9	3.5	5.122	1.128	9.5	25	5.624	3.33	10.5	7.5	16.226	3.934
9	4	5.105	1.148	9.5	30	4.859	3.581	10.5	8	16.214	3.94
9	4.5	5.085	1.167	10	0.5	11.118	2.874	10.5	8.5	16.202	3.948
9	5	5.062	1.185	10	1	11.116	2.889	10.5	9	16.189	3.958
9	5.5	5.037	1.204	10	1.5	11.113	2.916	10.5	9.5	16.175	3.969
9	6	5.01	1.224	10	2	11.11	2.94	10.5	10	16.16	3.983
9	6.5	4.98	1.245	10	2.5	11.105	2.958	10.5	15	15.973	4.215
9	7	4.948	1.268	10	3	11.099	2.971	10.5	20	15.711	4.495
9	7.5	4.914	1.293	10	3.5	11.091	2.981	10.5	25	15.375	4.721
9	8	4.878	1.32	10	4	11.083	2.99	10.5	30	14.965	4.892
9	8.5	4.839	1.35	10	4.5	11.074	2.997	11	0.5	23.934	4.685
9	9	4.797	1.383	10	5	11.063	3.004	11	1	23.933	4.697
9	9.5	4.754	1.419	10	5.5	11.052	3.01	11	1.5	23.932	4.719
9	10	4.708	1.457	10	6	11.039	3.016	11	2	23.93	4.738
9	15	4.131	1.936	10	6.5	11.025	3.023	11	2.5	23.928	4.752
9	20	3.39	2.4	10	7	11.011	3.031	11	3	23.925	4.762
9	25	2.621	2.788	10	7.5	10.995	3.04	11	3.5	23.922	4.769
9	30	1.973	3.132	10	8	10.978	3.05	11	4	23.918	4.774
9.5	0.5	7.583	1.906	10	8.5	10.959	3.062	11	4.5	23.913	4.778
9.5	1	7.581	1.924	10	9	10.94	3.075	11	5	23.908	4.782
9.5	1.5	7.577	1.958	10	9.5	10.92	3.091	11	5.5	23.903	4.785
9.5	2	7.571	1.988	10	10	10.898	3.11	11	6	23.897	4.788
9.5	2.5	7.564	2.012	10	15	10.624	3.398	11	6.5	23.891	4.791
9.5	3	7.555	2.03	10	20	10.241	3.726	11	7	23.884	4.794
9.5	3.5	7.545	2.044	10	25	9.751	3.989	11	7.5	23.877	4.798
9.5	4	7.532	2.057	10	30	9.163	4.194	11	8	23.869	4.803
9.5	4.5	7.519	2.068	10.5	0.5	16.31	3.804	11	8.5	23.86	4.809
9.5	5	7.503	2.08	10.5	1	16.309	3.816	11	9	23.851	4.817
9.5	5.5	7.486	2.091	10.5	1.5	16.307	3.84	11	9.5	23.842	4.826
9.5	6	7.468	2.102	10.5	2	16.304	3.861	11	10	23.832	4.837
9.5	6.5	7.448	2.115	10.5	2.5	16.301	3.876	11	15	23.704	5.039
9.5	7	7.426	2.128	10.5	3	16.297	3.887	11	20	23.526	5.289
9.5	7.5	7.403	2.143	10.5	3.5	16.292	3.895	11	25	23.296	5.49
9.5	8	7.378	2.16	10.5	4	16.286	3.902	11	30	23.016	5.638

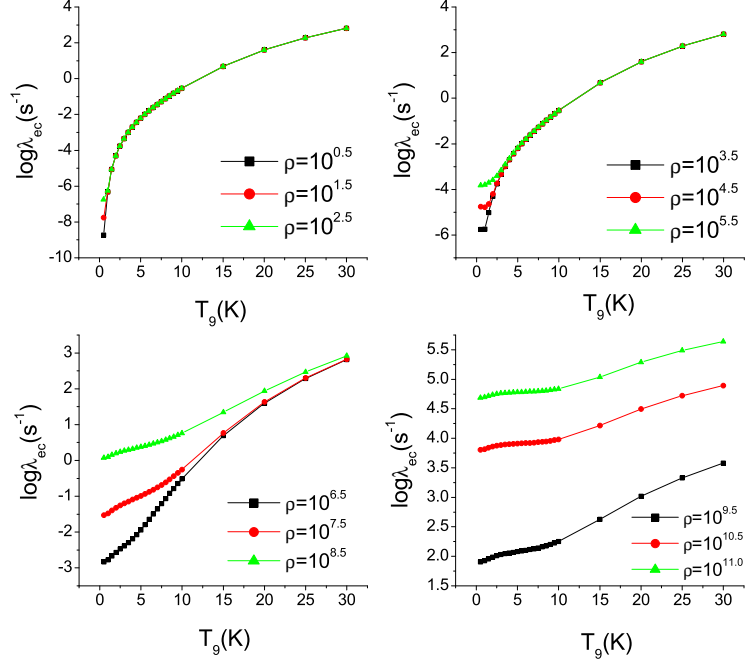


Figure 1: Electron capture rates on  $^{55}\text{Co}$ , as a function of temperature, for different selected densities. Densities are in units of  $g \text{ cm}^{-3}$ . Temperatures are measured in  $10^9 \text{ K}$  and  $\log \lambda_{ec}$  represents the log of electron capture rates in units of  $\text{sec}^{-1}$ .

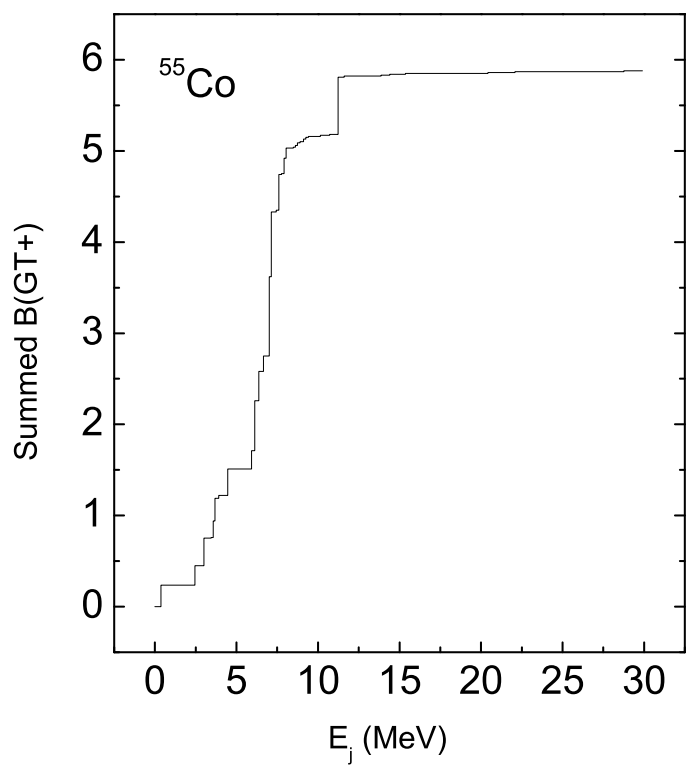


Figure 2: Cumulative sum of the B(GT) values. The energy scale refers to daughter excitation energies in <sup>55</sup>Fe.

This figure "fig1.JPG" is available in "JPG" format from:

<http://arxiv.org/ps/2505.01024v1>

This figure "fig2.JPG" is available in "JPG" format from:

<http://arxiv.org/ps/2505.01024v1>